Acta Cryst. (1996). A**52**, 812–829

Diffraction by Polycrystalline Fibers with Correlated Disorder

W. J. STROUD AND R. P. MILLANE*

Whistler Center for Carbohydrate Research and Computational Science and Engineering Program, Purdue University, West Lafayette, IN 47907-1160, USA. E-mail: rmillane@purdue.edu

(Received 3 January 1996; accepted 29 May 1996)

Abstract

Theory is developed for describing diffraction from polycrystalline fibers of helical molecules, in which the constituent crystallites contain correlated lattice disorder and uncorrelated substitution disorder. The theory utilizes a recently reported description of cylindrically averaged diffraction by distorted lattices that is based in real space and uses an imposed correlation field to describe correlated disorder [Stroud & Millane (1996). *Proc. R. Soc. London Ser. A*, **452**, 151–173]. The theory developed here is implemented as an efficient numerical algorithm for calculating diffraction patterns from fibers containing correlated disorder. Simulations are used to explore the effects of this kind of disorder and to characterize the disorder in a polynucleotide fiber whose diffraction pattern indicates its presence. This leads to a significant improvement in the agreement between the calculated and measured diffraction patterns over that from a model of only uncorrelated lattice disorder.

1. Introduction

X-ray fiber diffraction analysis is used to determine the molecular and crystal structures of polymers and rod-like macromolecular assemblies that can be prepared as oriented fibers or as rotationally disordered planar arrays (Arnott, 1980; Millane, 1988). The packing of molecules in fibers varies greatly, being ideally crystalline over small domains in the case of *polycrystalline* fibers to being random in the case of *non-crystalline* fibers. Calculation of diffraction patterns from both these types of fiber is straightforward. In an ideal polycrystalline fiber, the crystallites are randomly positioned and randomly rotated about an axis parallel to the long axes of the constituent molecules, so that the measured diffraction pattern consists of sharp Bragg reflections and is equivalent to the cylindrical projection of the diffraction pattern from a single crystal. In a non-crystalline fiber, the molecules are randomly positioned and rotated, and the diffraction pattern, which consists of intensity distributed continuously on layer lines, is equivalent to the cylindrical average of the diffraction pattern from an isolated molecule.

Some fibers, however, give diffraction patterns containing both sharp reflections and continuous intensity on layer lines (Miller & Parry, 1974; Arnott, 1980; Stroud & Millane, 1995*a*). The Bragg reflections are often confined to the center of the pattern, giving way to continuous layer-line intensities at high resolution. Specimens giving such patterns are essentially polycrystalline but the packing of the molecules in their crystallites is disordered in some way. Diffraction patterns of this kind have been used to determine structures by co-refining molecular and crystal structures against the continuous and Bragg diffraction (Arnott, Chandrasekaran, Millane & Park, 1986; Park, Arnott, Chandrasekaran, Millane & Campagnari, 1987), and treating the continuous intensity data as if from a non-crystalline fiber and the low-resolution Bragg data as if from an ideal polycrystalline specimen. Such an analysis is only approximately valid at best, since it ignores the effects of disorder on the diffracted intensities. Modeling disorder in polycrystalline fibers and quantifying its effect on diffraction is necessary for accurate structure determination using data from these kinds of pattern. Furthermore, identifying the kinds of disorder in a fiber may be important in its own right with regard to its relevance to the structure–function relationships of the molecules and the aggregates they form (Miller & Parry, 1974). The advent of methods for accurately measuring continuous diffraction data (Fraser, Macrae, Miller & Rowlands, 1976; Makowski, 1978; Millane & Arnott, 1986) affords the possibility of more fully utilizing diffraction data for this purpose.

Previously (Millane & Stroud, 1991; Stroud & Millane, 1995*a*,*b*), we reported an extension to several earlier descriptions of diffraction from polycrystalline fibers with *uncorrelated* disorder (Clark & Muus, 1962; Tanaka & Naya, 1969; Arnott, 1980). The disorder we considered consists of uncorrelated displacements of the molecules away from the positions they would occupy in an ordered crystallite, and uncorrelated variations in the orientations of the molecules about their long axes. The diffracted intensity calculated for fibers containing these forms of disorder separates into two distinct components: a set of Bragg reflections whose profiles are identical throughout reciprocal space and a set of continuous layer-line intensities. However, diffraction patterns measured from some disordered fibers do not appear to consist of distinct components of this kind. Rather, they show Bragg reflections that broaden with increasing resolution and merge into continuous diffraction at high

resolution (Hosemann & Bagchi, 1962). This is generally considered to result from correlated distortions of the crystal lattice (Alexander, 1969; Welberry, 1985; Fraser, Suzuki & Macrae, 1984). Incorporation of correlated lattice distortions into a model of polycrystalline fibers, and calculation of associated diffraction patterns, is the subject of this paper.

Two models of lattices with correlated distortions are the paracrystal (Hosemann & Bagchi, 1962) and the perturbed lattice (Welberry, Miller & Carroll, 1980; Welberry & Carroll, 1982, 1983). In the paracrystal model, a distorted lattice is generated by replacing vectors that form the edges of the unit cell of a periodic lattice with vectors that vary in both length and direction. Although construction of one-dimensional paracrystals is straightforward, two- and three-dimensional paracrystals cannot be constructed so readily; the principle difficulty being one of prescribing a joint probability distribution for the random lattice vectors that corresponds to stationary lattice statistics and is consistent with the constraint that the vectors describing the edges of each face of a distorted unit cell should add to zero so that there is closure of the face. The only paracrystal for which a method of construction has been determined is the so-called 'ideal paracrystal' (Hosemann & Bagchi, 1962). Each unit cell of an ideal paracrystal is a parallelepiped, so that the disorder is highly anisotropic and very restricted in form.

In contrast to the paracrystal, a perturbed lattice is specified by the statistics of the correlated displacements of its sites away from those of a *periodic reference lattice*, rather than the statistics of the relative positions of its sites. This produces a rather general description of lattice disorder and, since the random variables that describe the distorted lattice are the actual positions of the lattice sites, the problem of satisfying cell closure is circumvented. Generally, it is assumed that only random variables describing the positions of neighboring lattice sites interact, and that the statistics of the lattice perturbations are stationary. Determining joint density functions for the displacements of the vertices of a single unit cell that are consistent with these assumptions is difficult, however. Nonetheless, statistics for two classes of perturbed lattices have been determined. The statistics of lattices belonging to the class of perturbed lattices referred to as 'Gaussian growth disordered lattices' (Welberry, Miller & Carroll, 1980; Welberry & Carroll, 1982) are anisotropic, with correlations along the principal lattice axes decaying more slowly than those along the diagonals. Members of the second, more general, class of perturbed lattices, referred to as 'general symmetric Gaussian disordered lattices' (Welberry & Carroll, 1983), have more complex correlation structures and are capable of producing a greater variety of diffraction effects. In particular, the disorder statistics can be approximately isotropic over intermediate distances for appropriate choices for the short-range-disorder parameters. Calculating diffraction from both growth disordered and general symmetric Gaussian perturbed lattices is extremely intensive computationally, particularly for the latter class of lattices.

An alternative approach to formulating perturbed lattices, first adopted by de Graaf (1989), is to impose a correlation field on the lattice, rather than deriving it from nearest-neighbor statistics. The imposed field is assumed to at least approximate the actual field of a stationary model. We have recently developed this idea by formulating it in real space, rather than reciprocal space. For two-dimensional lattices, this allows the effect of correlated distortions both in and out of the plane to be described readily, and leads to an analytical expression that permits efficient calculation of the cylindrically averaged intensity diffracted by lattices with isotropic correlation fields of arbitrary form (Stroud & Millane, 1996). The calculated diffraction patterns reproduce the kinds of features (a gradual broadening of Bragg reflections with increasing resolution and blending into the continuous diffraction) seen on diffraction patterns from some polymer fibers (Stroud & Millane, 1996). This model appears, therefore, to be potentially useful for describing disorder in such fibers. It was developed (Stroud & Millane, 1996), however, for a lattice only (*i.e.* with a point scatterer at each lattice site). In order to apply this model to the analysis of polycrystalline fibers, we therefore further develop it here to include the presence of helical molecules at each lattice site. This involves two steps. The first is to replace the point scatterers at each site of the distorted lattice with helical molecules and the second is to incorporate *substitution* disorder (described in the next section), which allows random variations in the rotations of the molecules about their long axes as well as random variations in their directions.

In the next section, we outline our approach to this problem. The theory for calculating diffraction from polycrystalline fibers with correlated disorder is described in §3. Computational implementation of the theory is described in §4 and these methods are used to explore the effects of correlated disorder on diffraction patterns in §5. The model is used to characterize correlated disorder in a polynucleotide fiber in §6 and the implications of this work are discussed in the final section.

2. Preliminaries

A polycrystalline fiber can be modeled as a statistical ensemble of disordered crystallites formed by the aggregation of structurally regular segments of helical molecules. The crystallites are randomly rotated about their crystallographic c axes (chosen parallel to the helix axes of the molecules), which initially are treated as being oriented in a common direction referred to as the 'fiber axis'. The molecular segments forming the

crystallites are treated as being infinite in length so that the intensity diffracted by each crystallite is confined to a set of planes in reciprocal space. The intensity on a diffraction pattern is calculated by averaging the intensity diffracted by a crystallite over all disorder states and then cylindrically averaging this intensity to take into account the random orientation of the crystallites about their c axes. The result of this procedure is a set of layer-line intensities.

In a real specimen, the length of the structurally ordered segments of molecules that form crystallites, referred to as the *coherence length*, is finite, and the c axes of the crystallites have a range of orientations with respect to the fiber axis. Finite coherence length smears the layer-line intensities (calculated as described above) into bands parallel to the fiber axis and crystallite disorientation smears these bands along arcs centered on the origin of reciprocal space (Holmes & Barrington Leigh, 1974). The resulting two-dimensional diffraction pattern can be calculated from the layer-line intensities using equation (3*a*) of Holmes & Barrington Leigh (1974). We therefore focus our attention here on deriving expressions for these layer-line intensities, for a particular model of disordered crystallites.

The types of disorder considered here can be classified as *substitution disorder* and *lattice disorder*. Substitution disorder consists of variations in the kinds of unit at each lattice site or, since a single molecule in different orientations may be considered to be different units, variations in the disposition of a molecule at a lattice site. Lattice disorder consist of deviations in the positions of the molecules from their positions in an ordered crystal. The molecules are treated as rigid bodies that do not deform as a result of disorder.

We consider fibers in which the average crystallite structure can be described by a monoclinic unit cell (the c axis being the unique axis) containing one molecule. This describes many polycrystalline biopolymer fibers. In the absence of disorder, the long axes of the molecules intersect a plane normal to the fiber axis, at the sites of a two-dimensional periodic lattice described by the primitive lattice vectors **a** and **b**. Lattice disorder consists of distortions of this two-dimensional lattice into three-dimensional space. The coordinates of the positions of the lattice sites are treated as zero-mean random variables, and correlations between the displacements of different sites are described by an imposed isotropic correlation field (de Graaf, 1989; Stroud & Millane, 1996). Substitution disorder consists of rotations of the molecules about their long axes and variations in their direction ('up' or 'down'). Axial translations of the molecules may be treated as a component of substitution disorder, rather than of lattice disorder, if convenient (*i.e.* if doing so leads to a simpler description of the disorder). Lattice disorder and substitution disorder are treated as being independent of one another.

With cylindrical polar coordinates (R, ψ, Z) in reciprocal space, the layer-line intensities $I_l(R)$ diffracted from an ensemble of disordered crystallites can be written as (Suzuki, Fraser, Macrae & Rowlands, 1980; Stroud & Millane, 1995*a*)

$$I_l(R) = \langle\langle I(R, \psi, Z = l/c)\rangle_d\rangle_\psi, \tag{1}$$

where $I(R, \psi, Z)$ is the intensity diffracted from a single crystallite, $\langle\,\rangle_d$ denotes averaging over all states of disorder, $\langle\,\rangle_\psi$ denotes cylindrical averaging and c is the axial repeat distance of the molecules. In the next section, we develop (1) in detail for our model of correlated lattice disorder and uncorrelated substitution disorder.

3. Theory

The intensity diffracted by an ensemble of disordered, but oriented, crystallites can be written as (Stroud & Millane, 1995*a*)

$$I(\mathbf{R}) = \left\langle\left\langle \left| \sum_j \sum_k s_{\rm lat}(\mathbf{r}_{jk}) F_{jk}(\mathbf{R}) \times \exp[i2\pi\mathbf{R}\cdot(\mathbf{r}_{jk}+\mathbf{d}_{jk})] \right|^2 \right\rangle_d \right\rangle_\psi, \tag{2}$$

where $\mathbf{R}$ is the position vector in reciprocal space, $s_{\rm lat}(\mathbf{r}_{jk})$ is the shape function describing the cross-sectional shape of the crystallites in the lateral plane, $F_{jk}(\mathbf{R})$ is the structure factor of the molecule at the lattice site with indices (j, k) and $\mathbf{d}_{jk}$ is the displacement of this site away from its mean position $\mathbf{r}_{jk} = j\mathbf{a} + k\mathbf{b}$. The role of $s_{\rm lat}(\mathbf{r})$ here is to select sites from an infinite periodic reference lattice for inclusion in the finite crystallite.

As a result of substitution disorder, the structure factors $F_{jk}(\mathbf{R})$ vary from site to site. With the assumption that these variations are independent of the lattice disorder, averages over the structure factors can be calculated separately from those over variations in the $\mathbf{d}_{jk}$. For uncorrelated variations in the $F_{jk}(\mathbf{R})$,

$$\langle F_{jk}(\mathbf{R}) F^*_{j'k'}(\mathbf{R})\rangle_d = \begin{cases} \langle |F(\mathbf{R})|^2\rangle_d & \text{when } j = j' \text{ and } k = k' \\ |\langle F(\mathbf{R})\rangle_d|^2 & \text{otherwise.} \end{cases} \tag{3}$$

Separating the averages for lattice disorder and substitution disorder in (2) and substituting from (3) gives

$$I(\mathbf{R}) = N\left\{\langle\langle |F(\mathbf{R})|^2\rangle_d\rangle_\psi - \langle |\langle F(\mathbf{R})\rangle_d|^2\rangle_\psi\right\} + \left\langle |\langle F(\mathbf{R})\rangle_d|^2 \langle \mathcal{Z}(\mathbf{R})\rangle_d \right\rangle_\psi, \tag{4}$$

where N is the number of lattice sites in each crystallite and

$$\mathcal{Z}(\mathbf{R}) = \left| \sum_j \sum_k s_{\rm lat}(\mathbf{r}_{jk}) \exp[i2\pi\mathbf{R}\cdot(\mathbf{r}_{jk}+\mathbf{d}_{jk})] \right|^2 \tag{5}$$

is the interference function of the distorted lattice.

3.1. *Lattice disorder*

The interference function $\mathcal{Z}(\mathbf{R})$ describes diffraction from the distorted lattice that has point scatterers, rather than molecules, at its sites. For distortion vectors with stationary Gaussian statistics, the average of this function over all disorder states is given by (Stroud & Millane, 1996)

$$\langle \mathcal{Z}(\mathbf{R})\rangle_d = \sum_j \sum_k \exp(i2\pi\mathbf{R}\cdot\mathbf{r}_{jk}) \exp(-2\pi^2 \mathbf{R}\mathbf{C}_{jk}\mathbf{R}^T) \times \sum_{j'} \sum_{k'} s_{\text{lat}}(\mathbf{r}_{j+j',k+k'}) s_{\text{lat}}(\mathbf{r}_{j'k'}), \quad (6)$$

where $\mathbf{C}_{jk}$ is the covariance matrix of the components of the vector $(\mathbf{d}_{jk} - \mathbf{d}_{00})$, the superscript T denotes transposition and the vector $\mathbf{r}_{jk}$ is now an intersite vector so that $\mathbf{r}_{00} = \mathbf{0}$. The double summation in (6) over the indices j' and k' can be approximated as

$$\sum_{j'} \sum_{k'} s_{\text{lat}}(\mathbf{r}_{j+j',k+k'}) s_{\text{lat}}(\mathbf{r}_{j'k'}) \simeq t(\mathbf{r}_{jk})/A_{\text{cell}}, \quad (7)$$

where $t(\mathbf{r})$ is the autocorrelation of $s_{\text{lat}}(\mathbf{r})$ and $A_{\text{cell}} = |\mathbf{a}\times\mathbf{b}|$ is the area of the unit cell (Stroud & Millane, 1996). Equation (7) is exact in the limit of large crystallites and when both of its sides are averaged over all possible positions of the shape function relative to the reference lattice (Stroud & Millane, 1996). We include this averaging in the calculation of the diffracted intensity as it removes the arbitrary choice of an origin for the shape function, and for small crystallites it averages the intensity over small variations in the crystallite shapes, as defined by the actual lattice sites falling within the crystallite boundary, as will occur in a specimen. Substituting (7) into (6) then gives

$$\langle \mathcal{Z}(\mathbf{R})\rangle_d = (1/A_{\text{cell}}) \sum_j \sum_k t(\mathbf{r}_{jk}) \exp(-2\pi^2 \mathbf{R}\mathbf{C}_{jk}\mathbf{R}^T) \times \exp(i2\pi\mathbf{R}\cdot\mathbf{r}_{jk}). \quad (8)$$

Further development of this expression requires specification of the lattice-disorder statistics that determine the covariance matrix, $\mathbf{C}_{jk}$. Let (x, y, z) denote a Cartesian coordinate system in real space with the z axis parallel to the fiber axis and let $(d^x_{jk}, d^y_{jk}, d^z_{jk})$ denote the components of $\mathbf{d}_{jk}$ in this system. We assume that the components of $\mathbf{d}_{jk}$ are independent and that the covariances $\langle d^x_{jk} d^x_{00}\rangle$ and $\langle d^y_{jk} d^y_{00}\rangle$ are equal. The lateral and axial single site variances are defined as

$$\sigma^2_{\text{lat}} = \langle (d^x_{jk})^2\rangle = \langle (d^y_{jk})^2\rangle, \quad \sigma^2_{\text{axial}} = \langle (d^z_{jk})^2\rangle, \quad (9)$$

and the lateral and axial correlation functions as

$$\rho_{\text{lat}}(\mathbf{r}_{jk}) = \frac{\langle d^x_{jk} d^x_{00}\rangle}{\sigma^2_{\text{lat}}} = \frac{\langle d^y_{jk} d^y_{00}\rangle}{\sigma^2_{\text{lat}}}, \quad \rho_{\text{axial}}(\mathbf{r}_{jk}) = \frac{\langle d^z_{jk} d^z_{00}\rangle}{\sigma^2_{\text{axial}}}. \quad (10)$$

Following de Graaf (1989), we assume that correlations between the displacements of two sites depend only on their average separation $|\mathbf{r}_{jk}|$. Guided by the form of the correlation fields of Gaussian growth disordered lattices (Welberry, Miller & Carroll, 1980; Welberry & Carroll, 1982), we use circularly symmetric exponential correlation functions (Stroud & Millane, 1996)

$$\rho_{\text{lat}}(r) = \exp(-r/\eta_{\text{lat}}) \quad \text{and} \quad \rho_{\text{axial}}(r) = \exp(-r/\eta_{\text{axial}}), \quad (11)$$

where $r = |\mathbf{r}|$ and the constants η_{lat} and η_{axial} are correlation lengths. The exponential correlation fields of growth disordered lattices arise from the assumption that only molecules at neighboring sites interact. By choosing exponential correlation fields, we expect to retain some of the localized character of the interactions of a growth disordered system. Imposing isotropy constrains the number of parameters in the model and is consistent with the assumed circular symmetry of the marginal distributions of the displacement vectors.

Using (9), (10) and (11) to evaluate $\mathbf{C}_{jk}$ and substituting the result into (8) gives

$$\langle \mathcal{Z}(\mathbf{R})\rangle_d = (1/A_{\text{cell}}) \sum_j \sum_k t(\mathbf{r}_{jk}) w_{\text{lat}}(R, r_{jk}) w_{\text{axial}}(Z, r_{jk}) \times \exp(i2\pi\mathbf{R}\cdot\mathbf{r}_{jk}), \quad (12)$$

where

$$w_{\text{lat}}(R, r) = \exp\{-4\pi^2 R^2 \sigma^2_{\text{lat}}[1 - \rho_{\text{lat}}(r)]\} \quad (13)$$

is the lateral lattice disorder weight and

$$w_{\text{axial}}(Z, r) = \exp\{-4\pi^2 Z^2 \sigma^2_{\text{axial}}[1 - \rho_{\text{axial}}(r)]\} \quad (14)$$

is the axial lattice disorder weight. For a monoclinic system, the vectors $\mathbf{r}_{jk}$ all lie in a plane perpendicular to the fiber axis and hence the Z axis of reciprocal space, so that

$$\mathbf{R}\cdot\mathbf{r}_{jk} = R r_{jk} \cos(\psi - \varphi_{jk}), \quad (15)$$

where φ_{jk} is the angle between $\mathbf{r}_{jk}$ and the x axis. Substituting (15) into (8) allows the interference function to be written explicitly in terms of the reciprocal-space coordinates (R, ψ, Z) as

$$\langle \mathcal{Z}(R, \psi, Z)\rangle_d = (1/A_{\text{cell}}) \sum_j \sum_k t(\mathbf{r}_{jk}) \times w_{\text{lat}}(R, r_{jk}) w_{\text{axial}}(Z, r_{jk}) \times \exp[i2\pi R r_{jk} \cos(\psi - \varphi_{jk})]. \quad (16)$$

3.2. *Substitution disorder*

The terms in (4) affected by substitution disorder are $\langle F(\mathbf{R})\rangle_d$ and $\langle|F(\mathbf{R})|^2\rangle_d$. Evaluation of these terms differs depending on whether or not directional disorder is considered. Initially, we consider substitution disorder that does not involve directional disorder and defer consideration of the effects of directional disorder until §3.4.

The complex amplitude, $F_l(R,\psi)$, diffracted by a molecule with u_v symmetry (u repeats and v turns of the molecular helix in one c repeat) and infinite length is given by (Cochran, Crick & Vand, 1952; Klug & Franklin, 1958)

$$\begin{aligned} F_l(R,\psi) &= F(R,\psi,Z=l/c) \\ &= \sum_n G_{nl}(R)\exp[in(\psi+\pi/2)], \end{aligned} \tag{17}$$

where the $G_{nl}(R)$ are the *Fourier–Bessel structure factors* given by

$$G_{nl}(R) = \sum_j f_j(|\mathbf{R}|)\,J_n(2\pi R r_j)\exp[i(2\pi l z_j/c - n\varphi_j)], \tag{18}$$

where $J_n(x)$ is the nth-order Bessel function of the first kind, the sum over j is over all atoms in the helical repeat unit and $f_j(|\mathbf{R}|)$ is the scattering factor of the jth atom with cylindrical polar coordinates (r_j, φ_j, z_j). The summation in (17) is over all Bessel orders n satisfying the helix selection rule

$$l = um + vn, \tag{19}$$

where m is any integer.

It follows from (17) that the complex amplitude, $F_l'(R,\psi)$, diffracted by a molecule rotated through an angle φ about its long axis and translated along this axis by z, relative to a reference molecule with structure factors $G_{nl}(R)$, is given by

$$F_l'(R,\psi) = \exp(i2\pi zl/c)\sum_n G_{nl}(R)\exp[in(\psi-\varphi+\pi/2)]. \tag{20}$$

If $p(\varphi,z)\,\mathrm{d}\varphi\,\mathrm{d}z$ is the probability that the angular position of a molecule falls in the interval $(\varphi, \varphi+\mathrm{d}\varphi)$ and the axial position in the interval $(z, z+\mathrm{d}z)$, then (20) implies that (Stroud & Millane, 1995*a*)

$$\langle F_l(R,\psi)\rangle_d = \sum_n w_{nl}G_{nl}(R)\exp[in(\psi+\pi/2)], \tag{21}$$

where w_{nl}, the *substitution disorder weight*, is defined as

$$w_{nl} = \int_0^{c/u}\int_0^{2\pi} p(\varphi,z)\exp[i(2\pi zl/c - n\varphi)]\,\mathrm{d}\varphi\,\mathrm{d}z. \tag{22}$$

The limits in (22) correspond to the range of φ and z corresponding to distinguishable positions for a helical molecule with infinite coherence length. The probability density function $p(\varphi,z)$ should be suitably defined and normalized on this interval (Stroud & Millane, 1995*a*). The disorder weights w_{nl} are used to express the effects of substitution disorder. For a particular kind of disorder, $p(\varphi,z)$ can be determined and the w_{nl} calculated using (22). For example, explicit expressions for w_{nl} for random rotations, random axial translations and screw disorder are given in §3.6 of Stroud & Millane (1995*a*).

Use of (21) gives

$$\langle|\langle F_l(R,\psi)\rangle_d|^2\rangle_\psi = \sum_n |w_{nl}|^2|G_{nl}(R)|^2. \tag{23}$$

Similarly, it follows from (20) that

$$\langle\langle|F_l(R,\psi)|^2\rangle_d\rangle_\psi = \sum_n |G_{nl}(R)|^2, \tag{24}$$

which is independent of the substitution disorder.

3.3. *Combined lattice and substitution disorder*

The effects of correlated lattice disorder and uncorrelated substitution disorder are combined by substituting (16), (21), (23) and (24) into (4). This gives

$$\begin{aligned} I_l(R) &= \langle N\rangle\sum_n(1-|w_{nl}|^2)|G_{nl}(R)|^2 \\ &\quad + (1/A_{\text{cell}})\sum_j\sum_k\Big[t(\mathbf{r}_{jk})w_{\text{lat}}(R,r_{jk})w_{\text{axial}}(l/c,r_{jk}) \\ &\quad \times\sum_n\sum_m w_{nl}w_{ml}^*f_{jkmn}(R)G_{nl}(R)G_{ml}^*(R)\Big], \end{aligned} \tag{25}$$

where, because of the averaging of the diffracted intensity over all positions of the shape function relative to the reference lattice, N in (4) has been replaced by the corresponding average $\langle N\rangle$ given by

$$\langle N\rangle = \left\langle\sum_j\sum_k s(\mathbf{r}_{jk})\right\rangle = t(0)/A_{\text{cell}} = A_{\text{cryst}}/A_{\text{cell}}, \tag{26}$$

where A_{cryst} is the cross-sectional area of the crystallites. The function $f_{jkmn}(R)$ in (25) is defined as

$$\begin{aligned} f_{jkmn}(R) &= (1/2\pi)\int_0^{2\pi}\exp[i(n-m)(\psi+\pi/2)] \\ &\quad\times\exp[i2\pi Rr_{jk}\cos(\psi-\varphi_{jk})]\,\mathrm{d}\psi, \end{aligned} \tag{27}$$

which reduces to

$$f_{jkmn}(R) = J_{m-n}(2\pi Rr_{jk})\exp[i(n-m)\varphi_{jk}]. \tag{28}$$

Substituting (28) into (25) and simplifying gives

$$\begin{aligned} I_l(R) &= \langle N\rangle\sum_n|G_{nl}(R)|^2 + (1/A_{\text{cell}}) \\ &\quad\times\sum_j{\sum_k}'\Big[t(\mathbf{r}_{jk})w_{\text{lat}}(R,r_{jk})w_{\text{axial}}(l/c,r_{jk}) \\ &\quad\times\sum_n\sum_m J_{m-n}(2\pi Rr_{jk})\Re\{w_{nl}w_{ml}^*G_{nl}(R)G_{ml}^*(R) \\ &\quad\times\exp[i(n-m)\varphi_{jk}]\}\Big], \end{aligned} \tag{29}$$

where the notation $\sum_j \sum_k'$ denotes a double summation that excludes the term $j = k = 0$ and $\Re\{\ \}$ denotes the real part.

The first term in (29) represents the intensity diffracted by a non-crystalline fiber. The terms of the double summation modify this intensity and contribute to the sharp Bragg peaks. When there is significant lattice disorder, the lattice disorder weights approach 0 for large R and Z, the contribution of the the second term in (29) is small and the intensity approaches that diffracted by a non-crystalline fiber.

Calculating a diffraction pattern using (29) would appear to require the computationally expensive evaluation of many Bessel functions, both those that appear explicitly in (29) and those that are needed to calculate the Fourier–Bessel structure factors. Fortunately, the number of evaluations required is limited by the fact that, at any radius R, the only significant $G_{nl}(R)$ are those for which

$$|n| \lesssim 2\pi R r_{\max} + 2, \tag{30}$$

where $r_{\max}$ is the maximum radius of the molecule, are significant (Crowther, DeRosier & Klug, 1970; Makowski, 1982). If the summations over m and n are truncated accordingly, the functions $J_{m-n}(2\pi R r_{jk})$ need only be evaluated for m and n such that

$$|m - n| \lesssim 4\pi R r_{\max} + 4. \tag{31}$$

Additional savings in the number of computations are obtained when the effects of lattice and molecular symmetry are taken into account. Depending on the helix symmetry of the molecules and the rotational symmetry of the lattice, these savings can be considerable, as is described in §3.5.

3.4. *Directional disorder*

A crystallite contains directional disorder when the constituent molecules are randomly oriented either parallel or antiparallel to each other. We define a 'down' molecule as being generated from a reference 'up' molecule by a 180° rotation about the axis $(\varphi = \varphi_0, z = z_0)$. Directional disorder does not change the average $\langle\langle|F_l(R,\psi)|^2\rangle_d\rangle_\psi$ given by (24) (Stroud & Millane, 1995*a*). If up and down molecules are equally likely to occupy a lattice site, then (21) is replaced by

$$\langle F_l(R,\psi)\rangle_d = \sum_n w_{nl} H_{nl}(R) \exp[in(\psi + \pi/2)], \tag{32}$$

where

$$H_{nl}(R) = (1/2)\{G_{nl}(R) + G^*_{nl}(R) \times \exp[i(4\pi z_0 l/c - 2n\varphi_0)]\} \tag{33}$$

and the weights w_{nl} express the effects of any other forms of substitution disorder that occur along with the directional disorder. Substituting (32) into (4), along with (16) and (24), and evaluating the cylindrical averages gives

$$\langle I_l(R)\rangle = \langle N\rangle \sum_n |G_{nl}(R)|^2 + (1/A_{\text{cell}}) \times \sum_j \sum_k' \Big[t(\mathbf{r}_j) w_{\text{lat}}(R, r_{jk}) w_{\text{axial}}(l/c, r_{jk}) \times \sum_n \sum_m J_{m-n}(2\pi R r_{jk}) \Re\{w_{nl} w^*_{ml} H_{nl}(R) H^*_{ml}(R) \times \exp[i(n-m)\varphi_{jk}]\}\Big]. \tag{34}$$

Equation (34) is identical in form to (29) except that the $G_{nl}(R)$ are replaced by $H_{nl}(R)$ in the double summation.

3.5. *Effects of lattice and molecular symmetry*

Terms in (29) corresponding to vectors $\mathbf{r}_{jk}$ related by a symmetry of the undistorted lattice can be combined when the shape autocorrelation $t(\mathbf{r})$ shares this symmetry. This is ensured if $t(\mathbf{r})$ is circularly symmetric, as it is for crystallites that are circular in cross section. We assume that this is the case and write $t(\mathbf{r})$ as $t(r)$.

The four types of two-dimensional lattice to be considered (in decreasing order of symmetry) are hexagonal lattices, for which $a = b$ and $\gamma = 120°$ (γ being the angle between the average lattice vectors); square lattices, for which $a = b$ and $\gamma = 90°$; rectangular lattices, for which $a \neq b$ and $\gamma = 90°$; and oblique lattices (the remaining cases).

A hexagonal lattice has sixfold rotational symmetry. Combining terms in (29) corresponding to vectors $\mathbf{r}_{jk}$ related by this symmetry gives

$$I_l(R) = \langle N\rangle \sum_n |G_{nl}(R)|^2 + (1/A_{\text{cell}}) \times \sum_{j>0} \sum_{k=0}^{j-1} \Big[t(r_{jk}) w_{\text{lat}}(R, r_{jk}) w_{\text{axial}}(l/c, r_{jk}) \times \sum_n \sum_m J_{m-n}(2\pi R r_{jk}) \Re\Big\{ w_{nl} w^*_{ml} G_{nl}(R) G^*_{ml}(R) \times \sum_{p=0}^{5} \exp[i(n-m)(\varphi_{jk} + p\pi/3)]\Big\}\Big], \tag{35}$$

where the indices j and k are restricted to values corresponding to $\mathbf{r}_{jk}$ with $0 \leq \varphi_{jk} < \pi/3$. Since

$$\sum_{p=0}^{5} \exp[i(n-m)p\pi/3] = \begin{cases} 6 & \text{if } n-m \text{ is divisible by 6} \\ 0 & \text{otherwise,} \end{cases} \tag{36}$$

terms in (35) for which $n - m$ is not divisible by six vanish. Terms corresponding to $\mathbf{r}_{jk}$ that are related by

reflection in the line $\varphi = \pi/6$ can be combined and (35) rewritten as

$$I_l(R) = \langle N \rangle \sum_n |G_{nl}(R)|^2 + (1/A_{\text{cell}}) \times \sum_j \sum_k{}' \Big[t(r_{jk}) w_{\text{lat}}(R, r_{jk}) w_{\text{axial}}(l/c, r_{jk}) \times \sum_m \sum_n \Theta_{m-n}(\varphi_{jk}) J_{m-n}(2\pi R r_{jk}) \times \Re\{ w_{nl} w_{ml}^* G_{nl}(R) G_{ml}^*(R) \} \Big], \quad (37)$$

where

$$\Theta_p(\varphi) = \begin{cases} 6 & \varphi = 0 \text{ and } p \text{ is divisible by } 6 \\ 12\cos(p\varphi) & 0 < \varphi < \pi/6 \text{ and } p \text{ is divisible by } 6 \\ 6(-1)^{p/6} & \varphi = \pi/6 \text{ and } p \text{ is divisible by } 6 \\ 0 & \text{otherwise.} \end{cases} \quad (38)$$

The factor $\Theta_p(\varphi)$ is symmetric with respect to p, whereas $J_{-n}(x) = (-1)^n J_n(x)$, so that the only non-zero terms in (37) are those for which $m - n$ is divisible by 6 and therefore even. Consequently, the non-zero terms are symmetric under an interchange of m and n. Combining terms related by this symmetry gives

$$I_l(R) = \langle N \rangle \sum_n |G_{nl}(R)|^2 + (1/A_{\text{cell}}) \times \sum_j \sum_k{}' \Big[t(r_{jk}) w_{\text{lat}}(R, r_{jk}) w_{\text{axial}}(l/c, r_{jk}) \times \sum_n \sum_{m \geq n} \varepsilon_{mn} \Theta_{m-n}(\varphi_{jk}) J_{m-n}(2\pi R r_{jk}) \times \Re\{ w_{nl} w_{ml}^* G_{nl}(R) G_{ml}^*(R) \} \Big], \quad (39)$$

where ε_{mn} is defined as

$$\varepsilon_{mn} = \begin{cases} 1 & m = n \\ 2 & m \neq n. \end{cases} \quad (40)$$

If directional disorder is present, then $G_{nl}(R)$ is replaced by $H_{nl}(R)$ in the double summation in (39).

Following reasoning similar to that used above for hexagonal lattices shows that (39) is valid for the other classes of lattices but with $\Theta_p(\varphi)$ suitably redefined as follows: for square lattices,

$$\Theta_p(\varphi) = \begin{cases} 4 & \varphi = 0 \text{ and } p \text{ is divisible by } 4 \\ 8\cos(p\varphi) & 0 < \varphi < \pi/4 \text{ and } p \text{ is divisible by } 4 \\ 4(-1)^{p/4} & \varphi = \pi/4 \text{ and } p \text{ is divisible by } 4 \\ 0 & \text{otherwise;} \end{cases} \quad (41)$$

for rectangular lattices,

$$\Theta_p(\varphi) = \begin{cases} 2 & \varphi = 0 \text{ and } p \text{ is divisible by } 2 \\ 2(-1)^{p/2} & \varphi = \pi/2 \text{ and } p \text{ is divisible by } 2 \\ 4\cos(p\varphi) & 0 < \varphi < \pi/2 \text{ and } p \text{ is divisible by } 2 \\ 0 & \text{otherwise;} \end{cases} \quad (42)$$

and, for oblique lattices,

$$\Theta_p(\varphi) = \begin{cases} 2 & 0 \leq \varphi < \pi \text{ and } p \text{ is divisible by } 2 \\ 0 & \text{otherwise.} \end{cases} \quad (43)$$

The function $\Theta_p(\varphi)$ selects out a subset of the terms involving $J_{m-n}(2\pi R r_{jk})$ from (29) for inclusion in (39) so that significantly fewer of these terms need to be evaluated. In addition, the Bessel orders $m - n$ in (39) are restricted to values divisible by n_{rot}, the degree of rotational symmetry of the lattice, whereas those in (29) are not. Molecular symmetry further restricts the values of the Bessel orders as follows. Since m and n must both satisfy (19), their difference must be a multiple of u. If u is not divisible by n_{rot}, as may often be the case, then, for R within the resolution limit, few pairs of m and n satisfying the selection rule will also satisfy (31) and be divisible by n_{rot}. As the layer-line index l increases, the maximum value of R at which intensity is observed generally decreases so that the number of terms contributing to the intensity on the layer line decreases. In many cases, therefore, significantly fewer Bessel orders may need to be included in the calculation than expected.

For example, the molecule described in §5 has 11_1 helix symmetry, a maximum radius of approximately 12 Å and packs on a hexagonal lattice. For diffraction data out to 3 Å resolution, only those $G_{nl}(R)$ for which $|n| \leq 22$ are significant for $R \leq 0.33$ Å^{-1}, and only those orders for which $m - n$ is divisible by 6 are included in (39). As a result of the 11_1 symmetry, $m - n$ is always equal to a multiple of 11 and, except when $m = n$, $m - n$ is divisible by 6 only when the magnitude of either m or n is greater than or equal to 66. Consequently, only those terms in (39) for which $m = n$ contribute significantly to the diffraction pattern. Therefore, apart from the Bessel functions needed to calculate $G_{nl}(R)$, only the zero-order Bessel function $J_0(2\pi R r_{jk})$ must be evaluated for each value of R and r_{jk} when (39) is used to calculate the layer-line intensities. Overall, approximately 100 times fewer evaluations of $J_{m-n}(2\pi R r_{jk})$ terms are required using (39) instead of (29) in this case.

4. Computational methods

We have written software to calculate layer-line intensities using (39). The results presented in the following

two sections are generally for crystallites that are circular in cross section, for which

$$t(r) = 2r_c^2\kappa - r_c \sin\kappa, \tag{44}$$

where

$$\kappa = \cos^{-1}(r/2r_c) \tag{45}$$

and r_c is the radius of the crystallites. Our software accommodates both the case where the crystallites are all of the same size and the case where they vary in size. The effects of a distribution of crystallite radii are discussed in §5.1.

The calculation of intensity is performed in two stages by two independent programs. The first program analyzes the undistorted reference lattice and calculates the lengths, r_{jk}, and angles, φ_{jk}, of the unique intersite vectors from which all other intersite vectors can be generated by application of the rotation and mirror symmetries of the lattice. Many of the unique r_{jk} share the same φ_{jk}. A lookup table of the unique φ_{jk} is prepared so that all trigonometric terms in (39) need be calculated only once for each unique φ_{jk}. This table is written to a file, along with a table of the unique $\mathbf{r}_{jk}$, stored in terms of their lengths and the index of φ_{jk} in the angle lookup table and the values of $t(r_{jk})/A_{\text{cell}}$. This file is read and used by the second program, which calculates the layer-line intensities.

One potentially prohibitive aspect of the calculation of intensities using (39) is the necessity to calculate $J_n(2\pi R r_{jk})$ for many different r_{jk} and many R values in the interval $0 \le R \le R_{\max}$, where $R_{\max}$ is typically of the order of 0.3 Å^{-1} for a wide-angle fiber diffraction pattern. The problem is severe when r_c is large compared to the dimensions of the unit cell but can be alleviated by tabulating values $J_n(x)$ for samples of x spaced by $\Delta x = \pi/32$ over the range $0 \le x \le 4\pi R_{\max} r_c$ and calculating values of $J_n(x)$ for arbitrary x, as required, from the table, using linear interpolation. The chosen sample interval corresponds to 1/32 of the period of oscillation of $J_n(x)$ for large x and permits calculation of $J_n(2\pi R r_{jk})$ with a maximum error of approximately $\pm 6 \times 10^{-4}$. Decreasing the sample interval produces no discernible change in plots of the calculated amplitudes. The values of $J_n(2\pi R r_{jk})$ are stored in memory, which allows layer-line intensities for different disorders to be calculated rapidly.

The CPU time required to calculate a diffraction pattern varies, depending on the helix and lattice symmetries, the number of atoms in the helical repeat unit, the maximum radius of the molecule, the radius of the crystallites and the maximum reciprocal-space radius R. Some typical times for our software running on a Silicon Graphics Indy workstation with a 100 MHz R4000 processor and 32 Mbytes of memory, are shown in Table 1. Times are shown for calculating full diffraction patterns (all layer lines) out to 3 Å resolution for two molecules; a polynucleotide with 11_1 helix symmetry, and a polysaccharide with 2_1 symmetry. Approximately 90% of the reported times are consumed by initialization of the Bessel function lookup tables and calculation of the Fourier-Bessel structure factors. Subsequent calculations of patterns for different disorder parameters require only approximately 10% of the reported times. The reported times indicate the practicality of calculating diffraction patterns using the real space expressions for diffracted intensity developed here.

Table 1. *Computational times for calculation of all layer-line amplitudes out to 3.0 Å resolution, for crystallites with correlated lattice disorder*

Helix symmetry	Lattice*	No. of atoms per repeat unit	$r_{\max}$ (Å)	r_c	CPU time (s)
11_1	Hexagonal	61	12.0	5*a*	4.3
11_1	Hexagonal	61	12.0	20*a*	5.0
11_1	Oblique	61	12.0	5*a*	5.9
11_1	Oblique	61	12.0	20*a*	18
2_1	Hexagonal	18	3.3	5*a*	1.2
2_1	Hexagonal	18	3.3	20*a*	2.6
2_1	Oblique	18	3.3	5*a*	3.4
2_1	Oblique	18	3.3	20*a*	10

* For the oblique lattices, $a = b$ and $\gamma = 111°$.

5. Simulations

We have examined the effects of correlated disorder on diffraction from polycrystalline fibers by calculating diffraction patterns from model fibers incorporating various kinds of disorder. The molecule used in the calculations was the polynucleotide duplex poly(dA) · poly(rU), which has 11_1 helix symmetry and packs, on average, in a trigonal unit cell with $a = b = 24.8$ and $c = 33.7$ Å (Arnott, Chandrasekaran, Millane & Park, 1986). This molecule was also used in our study of the effects of uncorrelated lattice and substitution disorder (Stroud & Millane, 1995*a*). Its Fourier–Bessel structure factors were calculated from the published coordinates (Arnott *et al.*, 1986) using 'water-weighted' atomic scattering factors to model the effects of disordered water in the fiber. The calculated diffraction patterns are presented as plots of the diffracted amplitude $I_l^{1/2}(R)$ on each layer line as these plots show details more clearly than do continuous tone representations of full two-dimensional patterns.

The results are presented in the following two subsections. In the first, we investigate the effects of a distribution of crystallite sizes and compare our real-space calculation with previous reciprocal-space calculations and, in the second, we investigate the effects of different degrees of correlated disorder on diffraction patterns.

5.1. *Comparison of real- and reciprocal-space calculations*

Here we consider the effect of a distribution of crystallite sizes (which, of course, there will be in a real

fiber specimen) on the diffracted intensity and compare patterns calculated using the real-space expressions for intensity described in this paper with those calculated using the reciprocal-space expressions developed by us previously (Stroud & Millane, 1995*a*). Comparisons are made first for the case of no disorder and second for the case of uncorrelated disorder.

Fig. 1(*a*) shows the amplitude on the equator ($Z = 0$) for an ideal polycrystalline fiber (*i.e.* one with no disorder) with $r_c = 150$ Å calculated using (39). The pattern shows considerable oscillating diffuse intensity between the Bragg reflections, particularly at small values of R. These oscillations are not observed on measured diffraction patterns because of instrumental broadening effects and variations in crystallite size. The effect of instrumental broadening can be approximated by convoluting the calculated diffraction pattern with an appropriate point spread function, while that of varying crystallite size is described by averaging (29) over an appropriate distribution of crystallite sizes. The effect of this averaging is to replace $t(r)$ and N by their respective averages over the distribution of crystallite sizes. For circular crystallites, the shape autocorrelation function (44) is written as a function of r and r_c, the crystallite radius, and the average autocorrelation function calculated as

$$\langle t(r, r_c)\rangle = \int_0^\infty t(r, r_c)p(r_c)\,\mathrm{d}r_c, \qquad (46)$$

where $p(r_c)$ is the probability density function for circular crystallites of radius r_c. This integral is, in general, difficult to solve analytically but can readily be calculated numerically. The average of N is simply $\langle t(0, r_c)\rangle$. Fig. 1(*b*) shows a diffraction pattern calculated for a fiber with no disorder and circular crystallites, the radii of which vary according to a Gaussian distribution with mean 150 Å and standard deviation $\sigma_r = 20$ Å. The variation in crystallite size removes oscillations from the diffuse amplitude between the Bragg reflections and, as comparison of Figs. 1(*a*) and (*b*) shows, does so without removing this diffuse amplitude or significantly altering the widths of the Bragg reflections.

The diffuse amplitude appearing in Figs. 1(*a*) and (*b*) does not appear on patterns calculated in earlier studies of the effects of uncorrelated (Stroud & Millane, 1995*a*) and correlated (de Graaf, 1989) disorder on diffraction from fibers. In these earlier studies, the intensity diffracted from a fiber is expressed in reciprocal space as the sum of terms over the sites of the reciprocal lattice. Each term in the sum contains the Fourier transform of the shape autocorrelation function, which to facilitate calculation is approximated by a Gaussian 'profile' function. Fig. 1(*c*) shows the diffraction pattern calculated in reciprocal space using Gaussian profiles for a fiber with no disorder and $r_c = 150$ Å. Comparing Fig. 1(*c*) with Fig. 1(*a*) shows that this pattern reproduces the Bragg reflections in Fig. 1(*a*) but not the diffuse intensity. This is because the shape autocorrelation function corresponding to a Gaussian profile function differs from that given by (44).

The Gaussian profile function used to calculate Fig. 1(*c*) was previously derived using methods described by Guinier (1939) and Hosemann & Bagchi (1962), and is given by (Stroud & Millane, 1995*a*)

$$T'(R) = \pi^2 r_c^4 \exp(-\pi^2 r_c^2 R^2), \qquad (47)$$

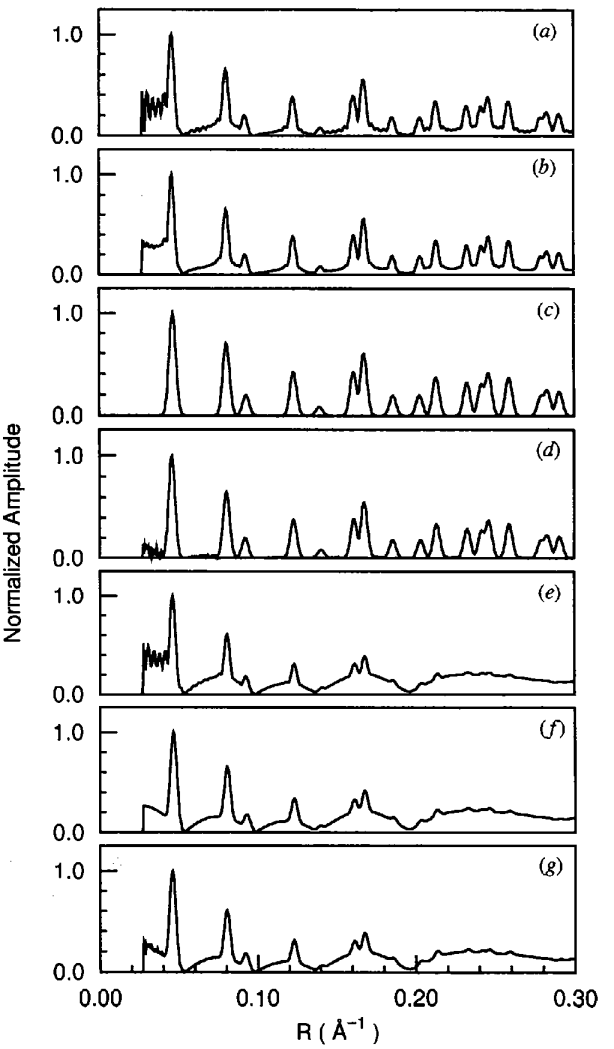

Fig. 1. Equatorial diffraction for an ideal polycrystalline fiber with $r_c = 150$ Å and: (*a*) calculated in real space for no disorder with $t(r)$ given by (44); (*b*) calculated in real space for no disorder and a Gaussian distribution of crystallite sizes with mean 150 Å and standard deviation 20 Å; (*c*) calculated in reciprocal space for no disorder; (*d*) calculated in real space for no disorder and $t(r)$ given by (47); (*e*) calculated in real space for uncorrelated lateral disorder with $\sigma_{lat} = 1.0$ Å and $t(r)$ given by (44); (*f*) calculated in reciprocal space for uncorrelated lateral disorder with $\sigma_{lat} = 1.0$ Å; (*g*) calculated in real space for uncorrelated lateral disorder with $\sigma_{lat} = 1.0$ Å and $t(r)$ given by (47).

the inverse Fourier transform of which is the shape autocorrelation function

$$t(r) = \pi^2 r_c^4 \exp(-r^2/r_c^2). \quad (48)$$

Calculating the intensity diffracted from a fiber with no disorder using (39) but with (48) rather than (44) as the shape autocorrelation function gives the diffraction pattern shown in Fig. 1(*d*). The diffuse amplitude at small R is computational noise resulting from the termination of the summation in (39) at a cutoff radius of $r = 6r_c$; a necessary measure since the shape autocorrelation function (48) does not fall to zero at a finite radius. Apart from this noise, the patterns in Figs. 1(*c*) and (*d*) are identical, indicating the equivalence of the description of diffraction developed here in real space and that developed previously in reciprocal space, at least for fibers with no disorder.

The differences between patterns calculated in real space and reciprocal space are less significant for disordered fibers. Figs. 1(*e*) and (*f*) show patterns for a fiber with uncorrelated disorder with $r_c = 150$ Å and $\sigma_{lat} = 1.2$ Å using the real-space and reciprocal-space expressions for the intensity, respectively. The diffuse amplitude in Fig. 1(*e*) has an oscillatory component that is quite significant at small R but is very small elsewhere. Repeating the real-space calculation but for a Gaussian shape autocorrelation function (47) gives the pattern in Fig. 1(*g*). Apart from some computational noise at small R, this pattern is identical to that in Fig. 1(*f*), demonstrating the equivalence of the real-space and reciprocal-space descriptions of diffraction for the case of uncorrelated disorder. The former description has the advantage, however, that it can incorporate correlated disorder. Treatment of correlated disorder in reciprocal space is very difficult. Comparison of Figs. 1(*e*) and (*g*) shows that they are virtually identical except for the oscillations in the diffuse intensity at small R. A distribution of crystallite sizes smooths the diffuse intensity at small R but otherwise has no effect on the calculated diffraction pattern. Conclusions regarding the general effects of disorder on fiber diffraction patterns can, therefore, safely be drawn from patterns calculated for a single crystallite size. This approach is adopted in §5.2.

5.2. *Effects of disorder on diffracted amplitudes*

In this section, we present a series of calculated diffraction patterns that illustrate the general effects of correlated disorder on diffraction from fibers. Fig. 2 shows a series of equatorial diffraction patterns calculated for fibers with $r_c = 150$ Å, $\sigma_{lat} = 1.2$ Å and η_{lat} ranging from 0 to 150 Å, as indicated in the figure caption. The diffraction pattern for uncorrelated disorder

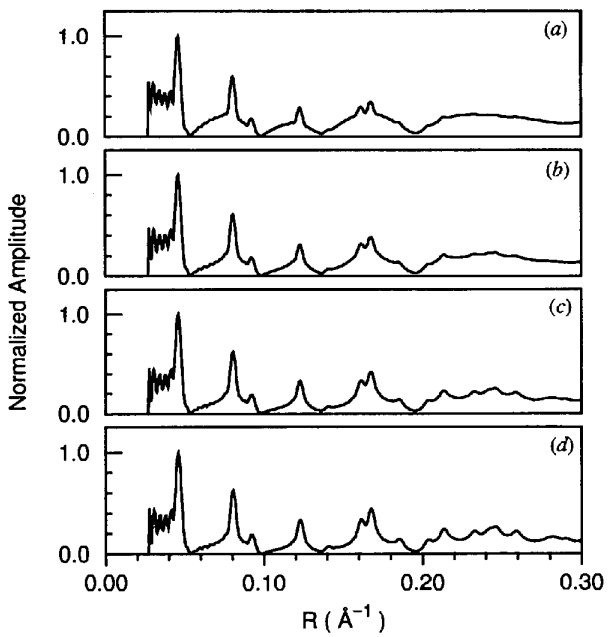

Fig. 2. Calculated equatorial diffraction with $r_c = 150$ Å, $\sigma_{lat} = 1.2$ Å and: (*a*) $\eta_{lat} = 0$; (*b*) $\eta_{lat} = 50$ Å; (*c*) $\eta_{lat} = 100$ Å; and (*d*) $\eta_{lat} = 150$ Å.

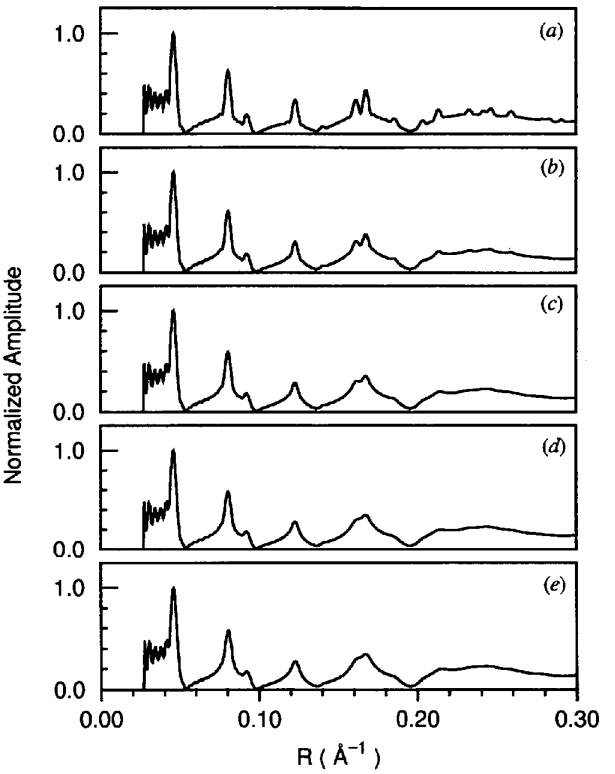

Fig. 3. Calculated equatorial diffraction with $r_c = 150$ Å, $\delta_{lat} = 1.0$ Å and: (*a*) $\sigma_{lat} = 0.8$ Å and $\eta_{lat} = 0$; (*b*) $\sigma_{lat} = 1.18$ Å and $\eta_{lat} = 40$ Å; (*c*) $\sigma_{lat} = 1.55$ Å and $\eta_{lat} = 80$ Å; (*d*) $\sigma_{lat} = 1.85$ Å and $\eta_{lat} = 120$ Å; and (*e*) $\sigma_{lat} = 2.11$ Å and $\eta_{lat} = 160$ Å.

(Fig. 2*a*) shows discrete reflections, which decrease in amplitude with distance from the origin, superimposed on a continuous background that shows the undulations of the molecular transform. When correlations are introduced, the distinction between Bragg and continuous amplitude is less clear (Figs. 2*b–d*). As η_{lat} increases, modulations that are the precursors of Bragg reflections appear in the continuous amplitude at large R while, closer to the origin, continuous amplitude is removed from between the Bragg reflections and concentrated to form broad bases for the reflections. Overall, the diffracted amplitude converges towards that for ordered crystallites as η_{lat} increases and the distortions of the lattice become more tightly correlated so that order is restored locally.

As we have noted previously (Stroud & Millane, 1996), the disorder parameters σ_{lat} and η_{lat} (and correspondingly σ_{axial} and η_{axial}) have opposing effects on the disorder in a crystallite with disorder increasing as σ_{lat} increases but decreasing as η_{lat} increases. The variance in the separation of neighboring lattice sites projected onto each of the principle lattice vectors **a**, **b** and **c**

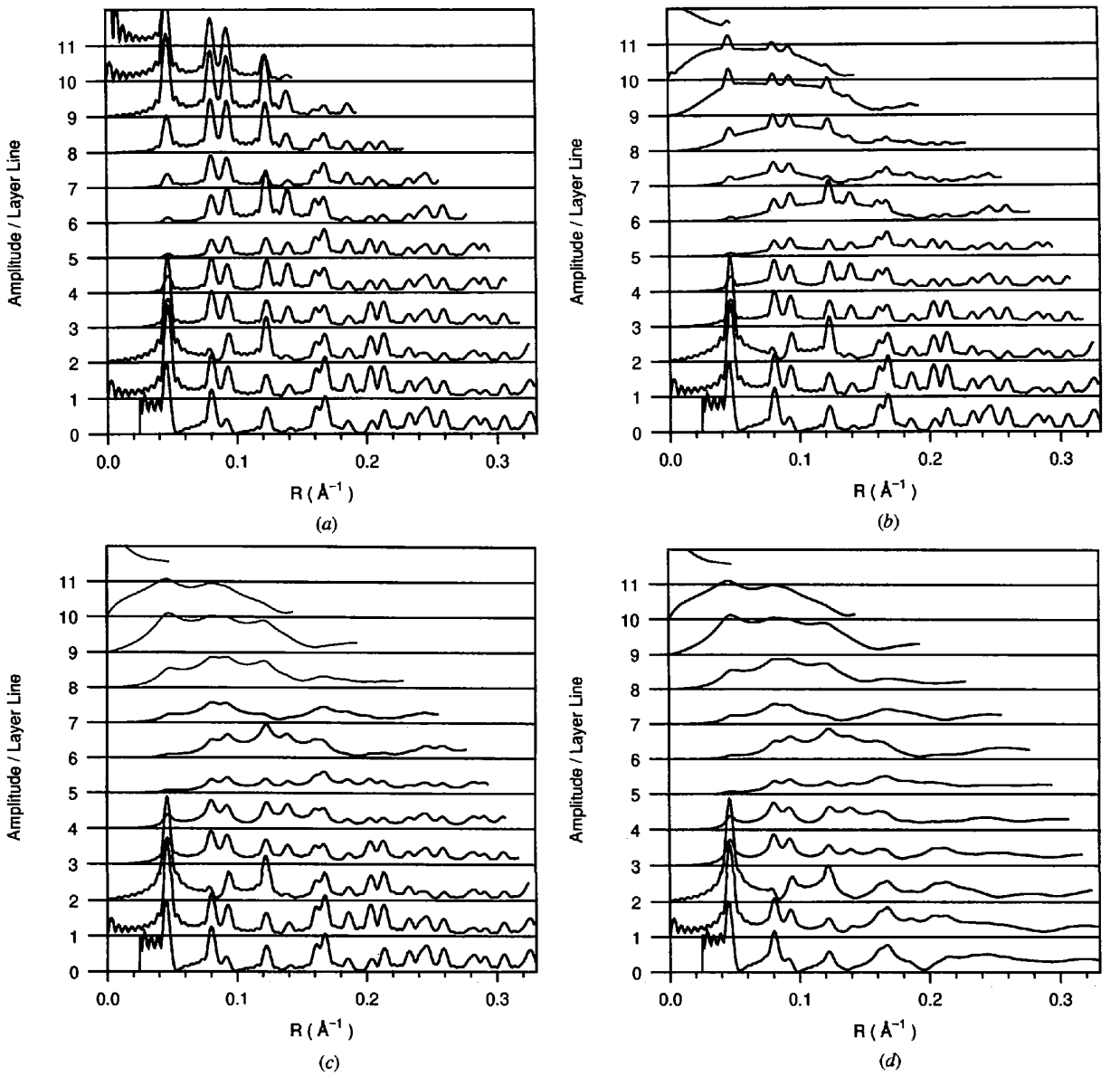

Fig. 4. Calculated diffraction patterns for a fiber with r_c = 100 Å and: (*a*) no disorder; (*b*) uncorrelated axial lattice disorder with σ_{axial} = 0.75 Å; (*c*) correlated axial lattice disorder with σ_{axial} = 1.6 Å and η_{axial} = 100 Å; and (*d*) correlated lateral and axial lattice disorder with σ_{lat} = σ_{axial} = 1.6 Å and η_{lat} = η_{axial} = 100 Å.

can be adopted as measures of local disorder (Stroud & Millane, 1996). For a hexagonal lattice with isotropic disorder, the variance in the lateral separation of nearest neighbors is the same whether projected along **a** or **b** and is denoted here as δ_{lat}^2. This variance is a strong determinant of the maximum reciprocal-space radius R out to which the interference effects of the lattice persist. Fig. 3 shows diffraction patterns calculated for $r_c = 150$ Å and $\delta_{\text{lat}} = 1.0$ Å, and σ_{lat} and η_{lat} as indicated in the caption. From the patterns, it is evident that, with δ_{lat} constant, reflections occur out to the same reciprocal radius once η_{lat} exceeds ~ 40 Å. As η_{lat} and σ_{lat} increase, however, the reflections at large R become broader and more rounded in appearance and merge into the continuous intensity. The Bragg reflections in the region $0.14 \lesssim R \lesssim 0.2$ Å^{-1} broaden and merge to form a crest. At small values of R, the diffraction patterns change only marginally. Increasing the value of δ_{lat} decreases the value of R at which reflection broadening is first evident, while decreasing δ_{lat} has the reverse effect.

The observations made above regarding the effects of lateral disorder also apply to those of axial disorder but with the effects extending in the direction of the Z axis. Fig. 4(*a*) shows the full diffraction pattern from a fiber with no disorder and Fig. 4(*b*) the pattern from a fiber with uncorrelated axial disorder with $\sigma_{\text{axial}} = 0.75$ Å and no lateral disorder. The uncorrelated axial disorder reduces the intensity of the reflections on the upper layer lines, without changing their widths, and introduces continuous intensity on these layer lines. The distinct Bragg and continuous components are clearly evident. Holding δ_{axial} constant and introducing correlations into the axial disorder produces the pattern shown in Fig. 4(*c*). Remnants of Bragg reflections still appear on the upper layer lines of this pattern but their profiles are much broader than those of reflections on the lower layer lines. Together, correlated lateral and axial lattice disorder give rise to diffraction patterns such as that in Fig. 4(*d*). The reflections in this pattern broaden with both increasing R and Z. Bragg reflections are completely absent from the periphery of this pattern and only small amounts of continuous intensity appear in its center.

The effects of substitution disorder have not been considered so far. Substitution disorder and lattice disorder are independent in the disorder model described here and, consequently, so are their effects on diffraction patterns. Substitution disorder by itself gives rise to diffraction patterns containing both Bragg reflections and continuous intensity, with the distribution of these two components in reciprocal space depending on the type of substitution disorder. Adding lattice disorder that is independent of the substitution disorder superimposes the weightings of lattice disorder onto those of substitution disorder, suppressing reflections where either the lateral or axial disorder weights are small and enhancing the continuous intensity in these regions. For example, Fig. 5(*a*) shows the diffraction pattern from a fiber in which the molecule at each lattice site adopts one of two positions, $(\varphi_i, z_i) = (0, 0)$ or $(270°, 0)$, with equal probability [the disorder weights for this kind of substitution disorder are given by equation (70) of Stroud & Millane (1995*a*)] but with no lattice disorder. The key feature of this disorder is the elimination of Bragg reflections from layer line $l = 2$ for $R < 0.18$ Å^{-1}. When lateral and axial correlated lattice disorder is added to the model (Fig. 5*b*), Bragg reflections are removed at high

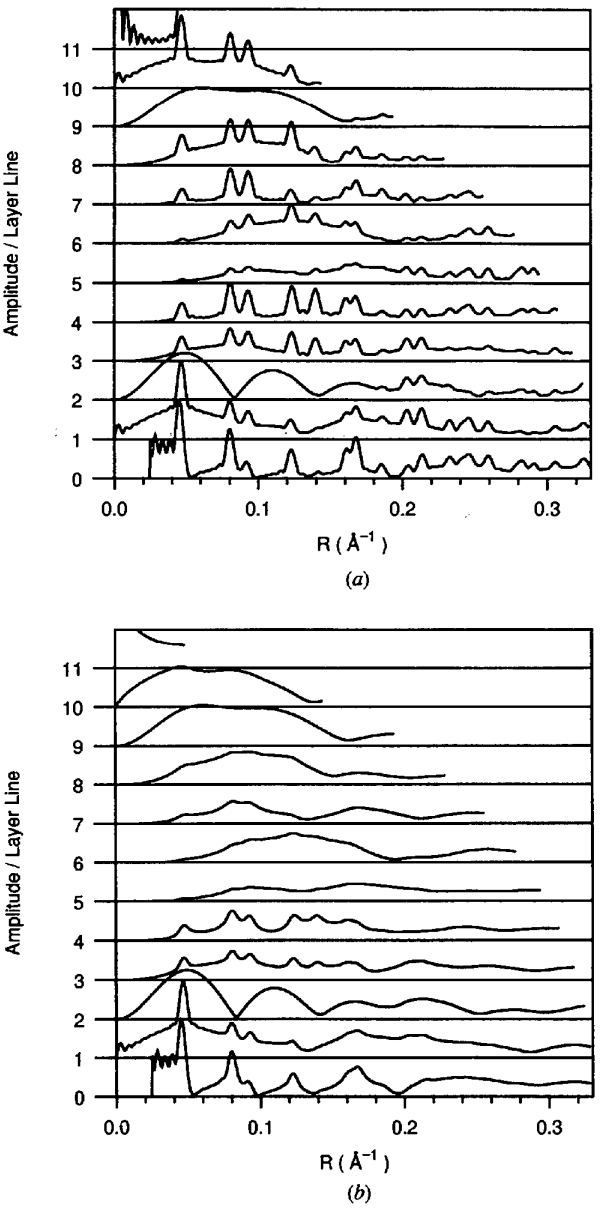

Fig. 5. Calculated diffraction patterns for a fiber with $r_c = 100$ Å and discrete rotations and translations with $(\varphi_i, z_i) = (0, 0)$ or $(270°, 0)$ and (*a*) no lattice disorder, (*b*) correlated lattice disorder with $\sigma_{\text{lat}} = \sigma_{\text{axial}} = 1.6$ Å and $\eta_{\text{lat}} = \eta_{\text{axial}} = 100$ Å.

resolution but the signature of the substitution disorder is still in evidence.

Fig. 6(*a*) shows a diffraction pattern from a fiber with random screw disorder and no lattice disorder, while Fig. 6(*b*) shows the pattern from a screw-disordered fiber with correlated lattice disorder. The principle effect of random screw disorder is the removal of sharp reflections from the upper layer lines close to the Z axis. When lattice disorder is introduced, this effect is not altered, although it is less clearly in evidence since the lattice disorder weakens the reflections unaffected by the screw disorder and completely removes the reflections at large values of R.

Fig. 7 shows continuous tone representations of the amplitudes in one quadrant of the full diffraction patterns calculated from the layer-line amplitudes shown in Fig. 5. These patterns are calculated as described in §4 of Stroud & Millane (1995*a*) for a disorientation angle

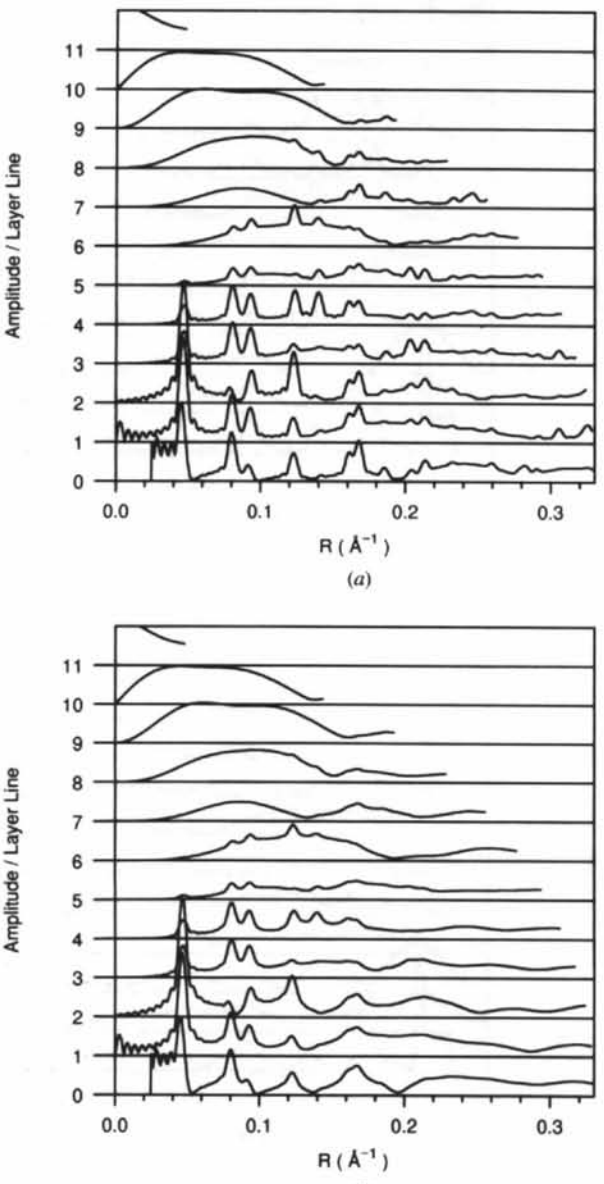

Fig. 6. Calculated diffraction patterns for a fiber with $r_c = 100$ Å and random screw disorder and (*a*) no lattice disorder, (*b*) correlated lattice disorder with $\sigma_{lat} = \sigma_{axial} = 1.6$ Å and $\eta_{lat} = \eta_{axial} = 100$ Å.

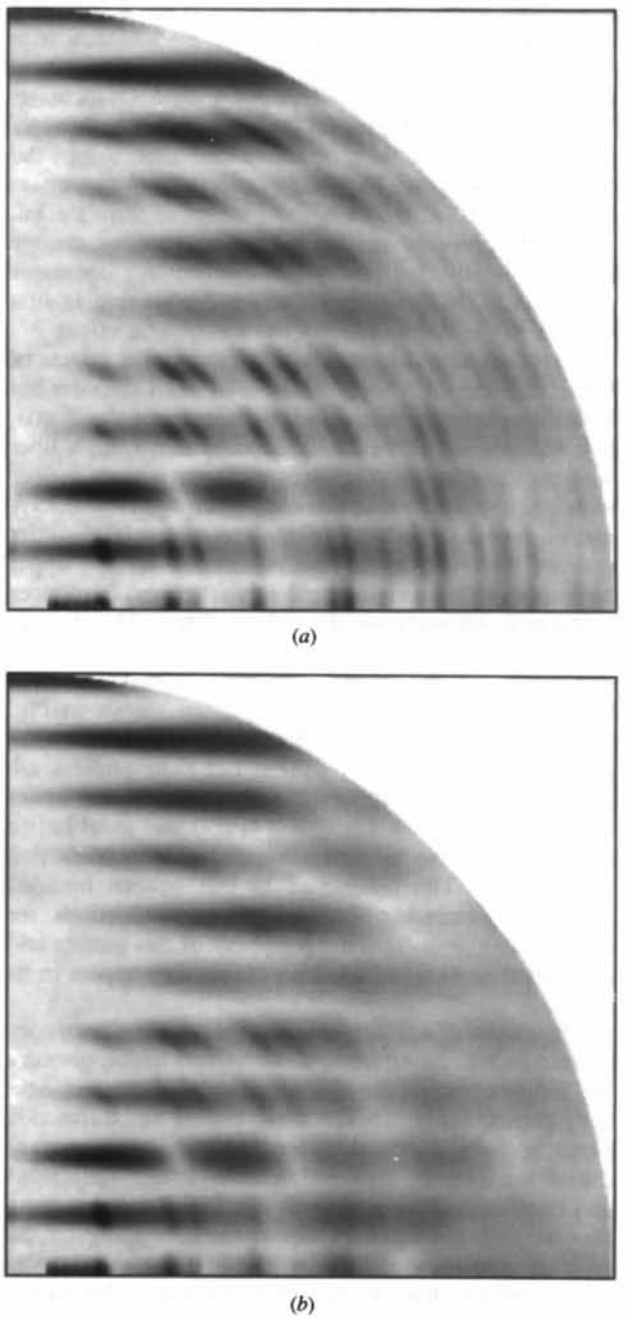

Fig. 7. Calculated full diffraction patterns for a fiber with $\sigma_0 = 2°$ and $l_c = 200$ Å, discrete rotations and translations with $(\varphi_i, z_i) = (0, 0)$ or $(270°, 0)$ and (*a*) no lattice disorder, (*b*) lattice disorder with $\sigma_{lat} = \sigma_{axial} = 1.6$ Å and $\eta_{lat} = \eta_{axial} = 100$ Å.

$\alpha_0 = 2°$ and a coherence length $l_c = 200$ Å. These figures illustrate the effects of disorder as they would be seen in two-dimensional measured diffraction patterns mapped into reciprocal space.

6. Analysis of correlated disorder in a polynucleotide fiber

Previously, we analyzed a diffraction pattern from a fiber of poly(dA) · poly(rU) in terms of uncorrelated lattice disorder and substitution disorder using the reciprocal-space description of the effects of this disorder and adjusting the disorder parameters so as to optimize the agreement between the calculated and measured diffraction (Stroud & Millane, 1995*b*). The observed diffraction was explained in terms of a model containing uncorrelated lattice disorder and substitution disorder consisting of small rotations of the molecules about their long axes. However, as we noted previously, the distribution of intensity on the equator of the measured diffraction pattern indicates that the lateral lattice disorder in the specimen may be correlated (Stroud & Millane 1995*b*). The amplitude on layer lines other than the equator (see Fig. 6 of Stroud & Millane 1995*b*) is mainly continuous and the slight broadening of the reflections that remain, with increasing Z, can be attributed to the effects of finite coherence length and crystallite disorientation rather than to correlated axial lattice disorder (Stroud & Millane, 1995*b*). In this section, we extend our earlier analysis of diffraction from poly(dA) · poly(rU) by including correlations in our description of lattice disorder and estimate the parameters of the model by matching the calculated and measured equatorial diffraction. This leads to a superior match between the calculated and observed reflection profiles.

A trace of the diffracted amplitude on the equator of the measured pattern is shown in Fig. 8(*a*). This trace shows four Bragg reflections in the region $R < 0.14$ Å^{-1} that broaden and give way to continuous amplitude at higher resolution, with a distinct crest in the continuous amplitude appearing at $R \simeq 0.16$ Å^{-1}. The disorder parameters estimated previously (Stroud & Millane, 1995*b*) for the uncorrelated model are as follows: $r_c = 100$ Å, $\sigma_{\text{lat}} = \sigma_{\text{axial}} = 1.2$ Å, rotational disorder with $\sigma_\varphi = 30°$. Calculated layer-line amplitudes were corrected for the effects of crystallite disorientation with $\alpha_0 = 3°$, coherence length $l_c = 175$ Å and a Gaussian beam profile with a standard deviation $\sigma_{\text{beam}} = 8 \times 10^{-4}$ Å^{-1}. The equatorial diffraction for these parameters, calculated using (39), is shown in Fig. 8(*b*). This pattern matches the observed pattern in that Bragg reflections are eliminated from the region $R \gtrsim 0.17$ Å^{-1} with the crest at $R \simeq 0.16$ Å^{-1} being interpreted as the vestige of two Bragg reflections. The discrepancy between the relative amplitudes of the Bragg reflections at $R \simeq 0.046$ and $R \simeq 0.08$ Å^{-1} on the observed and calculated patterns has been discussed previously (Stroud & Millane, 1995*b*) and is thought to be due either to small errors in the molecular transform or to the presence of organized water or ions that increase the effective radius of the molecule. The relative amplitude of these two reflections is not, however, affected by disorder (Stroud & Millane, 1995*b*). The pattern in Fig. 8(*b*) differs from that in Fig. 8(*a*) in two other respects. First, the continuous amplitude on the calculated pattern produces shoulders on the Bragg reflections, particularly on the low-resolution sides of the reflections at $R \simeq 0.08$ and $R \simeq 0.12$ Å^{-1}, whereas the continuous intensity on the measured pattern blends into the Bragg reflections. And, second, the Bragg reflections on the calculated pattern are constant in width, whereas those on the measured pattern broaden with increasing R. Both these discrepancies indicate the presence of correlated disorder in the specimen.

To help compensate for any errors in the molecular transform, and to aid detailed comparison of the measured and calculated reflection profiles, we divide the equator into four regions and normalize the calculated and observed amplitude in these regions to the respective peak amplitudes. The resulting measured amplitudes are shown as broken lines in Figs. 9(*a*)–(*d*), along with the amplitudes calculated using the model with uncorrelated disorder, which are shown as solid lines. Comparison of the measured and calculated amplitudes in Figs. 9(*a*)–(*d*) shows the discrepancies described above. The broad shoulders on the bases of the Bragg reflections calculated from the model are particularly evident in Figs. 9(*b*) and

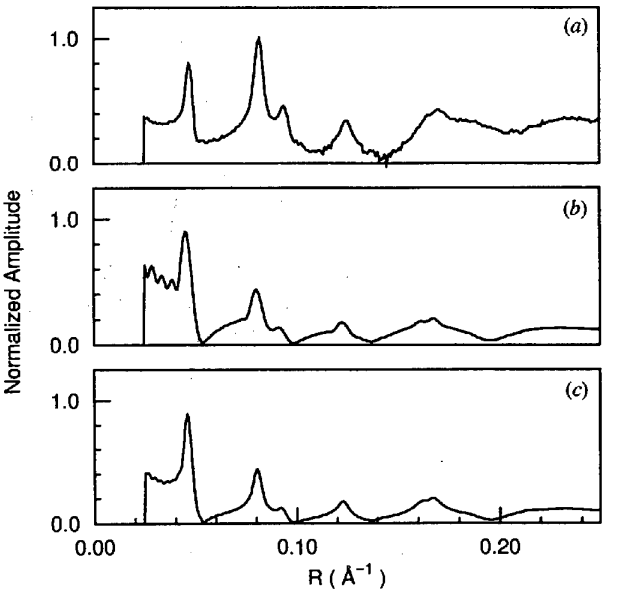

Fig. 8. Equatorial diffracted amplitude from poly(dA) · poly(rU): (*a*) measured; (*b*) calculated for uncorrelated lattice disorder with $\sigma_{\text{lat}} = 1.2$ Å, rotational disorder with $\sigma_\varphi = 30°$ and $r_c = 100$ Å, $l_c = 175$ Å, $\alpha_0 = 3°$ and $\sigma_{\text{beam}} = 8 \times 10^{-4}$ Å^{-1}; and (*c*) calculated for correlated lattice disorder with $\sigma_{\text{lat}} = 1.9$ Å, $\eta_{\text{lat}} = 125$ Å, $\langle r_c \rangle = 160$ Å, $\sigma_r = 20$ Å and σ_φ, l_c, α_0 and σ_{beam} as in (*b*).

(*c*). The calculated and observed reflections in Fig. 9(*b*) match in width, whereas the calculated reflection in Fig. 9(*a*) is broader than the observed reflection. This results from the inability of a model with uncorrelated disorder to describe peak broadening. Our goal is to see if these discrepancies can be explained by correlated distortions of the lattice.

Since the parameters σ_{lat}, η_{lat} and r_c together determine the shapes of the Bragg reflections when correlations are introduced by increasing η_{lat} away from zero, the parameters σ_{lat} and r_c must also be adjusted. A survey of the equatorial diffraction for a range of values for these three parameters showed that the values $\sigma_{lat} = 1.9$ Å, $\eta_{lat} = 125$ Å and $r_c = 160$ Å gave the

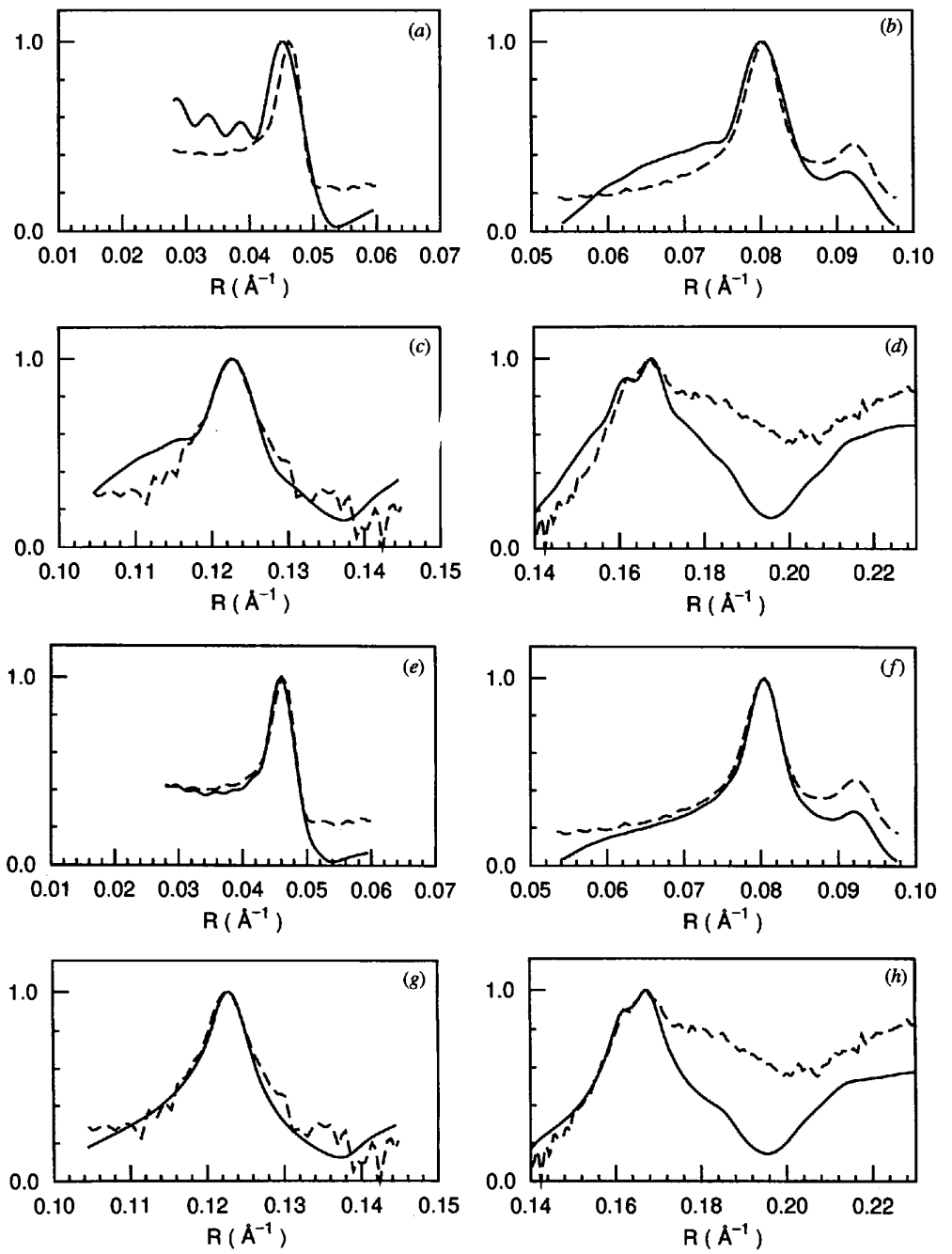

Fig. 9. Observed (– – –) and calculated (——) normalized amplitude in different regions of the equator for uncorrelated disorder (*a*)–(*d*) and correlated disorder (*e*)–(*h*) with parameters as listed in the caption to Fig. 8.

best agreement between the measured and calculated amplitudes (Figs. 9*e–h*). The parameters α_0, l_c and σ_{beam} were fixed at the values given above. A variation in crystallite size with $\sigma_r = 20$ Å was needed in order to remove excessive oscillations from the calculated amplitude in the region $R \lesssim 0.04$ Å^{-1}. This variation does not significantly alter the width of the Bragg reflections.

Previously, we estimated the crystallite radius as $r_c = 100$ Å in order to approximately match the widths of all the reflections calculated from the model with uncorrelated disorder with those of the reflections on the observed pattern. The smaller crystallite size resulted from our attempt to match the broader reflections at higher resolutions, the cost being that the calculated low-resolution reflections were then too broad. Correlated disorder, however, reproduces the reflection broadening with increasing resolution, making it possible to match the widths of both high- and low-resolution calculated reflections to those observed. The larger estimate of crystallite radius made here improves the width of the reflection at $R \simeq 0.045$ Å^{-1} and, because of the steep slope of the molecular transform in the vicinity of this reflection, shifts the reflection towards the position of the observed reflection. The correlations in the lattice disorder remove the shoulders from the bases of the Bragg reflections at $R \simeq 0.08$ and $R \simeq 0.12$ Å^{-1}, greatly extending the range over which there is agreement between the calculated and measured amplitudes in Figs. 9(*f*) and (*g*). The leading edge of the crest at $R \simeq 0.16$ Å^{-1} is better matched by the continuous amplitude of the correlated model, but the trough at $R \simeq 0.19$ Å^{-1} remains. This trough occurs in the molecular transform and is not a product of interference from the disordered lattice. Overall then, the incorporation of correlated lattice disorder substantially improves the agreement between the calculated and measured equatorial diffraction.

It is interesting to note that $\delta_{lat} = 1.7$ Å for both the model with uncorrelated disorder and the model with correlated disorder. Both models predict, therefore, the same degree of short-range order in the specimen, but differ in their description of long-range order; the model that includes correlations giving the best description.

7. Discussion

The description of diffraction from disordered polymer fibers presented here is an extension of both our earlier model of uncorrelated disorder in fibers (Stroud & Millane, 1995*a*) and our description of cylindrically averaged diffraction from lattices with correlated lattice disorder (Stroud & Millane, 1996). In formulating the latter, we adopted an approach based on a summation of terms over the sites of a lattice in real space. This approach has several advantages over a convolution-based description in reciprocal space (de Graaf, 1989); it allows cylindrical averaging of the intensity to be performed analytically; it yields an equation for the diffracted intensity that allows layer-line intensities to be calculated at a lower computational cost; and it removes restrictions from the types of correlation fields for which calculation of diffraction patterns is feasible. This leads to a very flexible model into which other features, such as a distribution of crystallite sizes, are easily incorporated.

In this paper, we have included molecules at the sites of the distorted lattice, included substitution disorder and obtained an expression for the cylindrically averaged intensity. When the average symmetry of the distorted lattice and the interaction between this symmetry and the helix symmetry of the molecules are taken into account, significant reductions in the number of calculations required to compute a fiber diffraction pattern using this expression are realized.

Diffraction patterns calculated for fibers with correlated lattice disorder show Bragg reflections that broaden with distance from the origin of reciprocal space. The correlations permit the distribution of intensity at the periphery of a pattern to be manipulated without altering the distribution of intensity at the center. Without correlations, the transition from Bragg to continuous intensity is controlled by just two lattice disorder parameters, σ_{lat} and σ_{axial}. Making these parameters large removes Bragg reflections from the periphery of a diffraction pattern but introduces considerable continuous intensity at its center. With correlated disorder, however, it is possible to eliminate Bragg reflections from the periphery of a pattern without introducing significant continuous intensity at the center (as is seen in many fiber diffraction patterns) by varying the disorder parameters in such a manner that the variances in the lateral and axial separations of neighboring molecules are not changed. Reflections at intermediate resolutions do, however, then broaden in consequence. This broadening is most pronounced when δ_{lat} and δ_{axial} are at least of order $0.04a$, and η_{lat} and η_{axial} are approximately equal to r_c; that is, when there are large lattice distortions that are tightly coupled over the entire crystallite. Such disorder is reminiscent of that in a paracrystal. The difference here, however, is that the disorder is isotropic.

The calculated patterns presented here show that correlated axial shifts of the molecules cause reflections to broaden with distance from the equator. They are not, however, the only source of this broadening. We have shown previously that crystallite disorientation and coherence length effects can significantly broaden Bragg reflections on the upper layer lines of a fiber diffraction pattern by smearing intensity along the layer line, while at the same time reducing their peak intensities (Stroud & Millane, 1995*b*). This broadening differs from that produced by disorder, however, in that reflections closest to the meridian are broadened more than those removed from it. The widths of the layer lines on a recorded pattern and the extent of angular arcing of the

reflections indicate the contribution that disorientation and coherence length make to reflection broadening.

Reflection profiles are determined by both the transform of the autocorrelation of the crystallite-shape function and the transform and self-convolution properties of the correlation fields. This is not directly evident in the current formulation but is evident in the reciprocal-space description of diffraction from distorted lattices (de Graaf, 1989; Stroud & Millane 1996). Changing the correlation field changes both the profiles of the reflections at low resolution and the broadening of reflections with increasing R and Z. Correlation fields other than the exponential fields considered here will alter the details of reflection broadening and may influence the distribution of continuous intensity in the low-resolution region of a diffraction pattern. For the exponential correlation fields chosen here, reflection broadening initiates at the base of the reflection and, as a result, continuous intensity appears between reflections at low resolution, even though the reflections are well resolved. This is evident in all of the patterns in Fig. 4, particularly on the equator where the reflections at $R \simeq 0.08$ and $R \simeq 0.12\,\text{Å}^{-1}$ have extended tails on their low-resolution sides. These tails are evident in the diffraction pattern calculated for a lattice with no disorder (Fig. 4*a*) and are, therefore, also related to the shape autocorrelation function used.

The current model includes the description of substitution disorder developed previously (Stroud & Millane, 1995*a*). Since substitution disorder and lattice disorder are treated as being independent, the effects of substitution disorder are the same for correlated lattice disorder as they are for uncorrelated lattice disorder. One possible extension of the disorder model presented here would be to allow for coupling between substitution disorder and lattice disorder. Formulating a general description of this coupling is likely to be very difficult for the general case, if it is indeed possible at all. Such coupling would in general arise from specific interactions between molecules that, because of substitution disorder, would vary between different pairs of adjacent molecules, leading to difficulties in formulating a general description of coupling between the two types of disorder. Detailed molecular models might, however, be used to investigate relationships between lattice and substitution disorder for specific systems. It should also be possible to combine the description of diffraction developed here with a description of the effects of correlated (cumulative) disorder *within* the molecules (Barakat, 1987; Inouye, 1994).

Comparison of the observed equatorial amplitude diffracted from a fiber of poly(dA)·poly(rU) and that calculated from our model shows that introducing correlations significantly improves the match between the calculated and observed patterns. This is not an overall improvement due to an additional parameter in the model but an improvement in the character of particular features of the calculated pattern that leads to a much better match with the data. This indicates that the disorder model is consistent with the diffraction data from the biopolymer fiber considered and is probably, therefore, an appropriate model for other fiber specimens with diffraction patterns that show evidence of correlated lattice disorder. As shown here, matching calculated and measured diffraction patterns allows disorder parameters to be estimated and it may be possible to modify procedures for structure determination so that they take into account the effects of correlated disorder.

Supported by the US National Science Foundation (MCB-9219736 to RPM).

References

Alexander, L. E. (1969). *X-ray Diffraction Methods in Polymer Science*. New York: Wiley-Interscience.

Arnott, S. (1980). *Fiber Diffraction Methods*, edited by A. D. French & K. H. Gardner, pp. 1–30. *ACS Symposium Series*, Vol. 141. Washington: American Chemical Society.

Arnott, S., Chandrasekaran, R., Millane, R. P. & Park, H. (1986). *J. Mol. Biol.* **188**, 631–640.

Barakat, R. (1987). *Acta Cryst.* A**43**, 45–49.

Clark, E. S. & Muus, I. T. (1962). *Z. Kristallogr.* **117**, 108–118.

Cochran, W., Crick, F. H. C. & Vand, V. (1952). *Acta Cryst.* **5**, 581–586.

Crowther, R. A., DeRosier, D. J. & Klug, A. (1970). *Proc. R. Soc. London Ser. A*, **317**, 319–340.

Fraser, R. D. B., Macrae, T. P., Miller, A. & Rowlands, R. J. (1976). *J. Appl. Cryst.* **9**, 81–94.

Fraser, R. D. B., Suzuki, E. & Macrae, T. P. (1984). *Structure of Crystalline Polymers*, edited by I. H. Hall, pp. 1–37. New York: Elsevier.

Graaf, H. de (1989). *Acta Cryst.* A**45**, 861–870.

Guinier, M. A. (1939). *Ann. Phys. (Leipzig)*, **12**, 161–237.

Holmes, K. C. & Barrington Leigh, J. (1974). *Acta Cryst.* A**30**, 635–638.

Hosemann, R. & Bagchi, S. N. (1962). *Direct Analysis of Diffraction by Matter*. Amsterdam: North-Holland.

Inouye, H. (1994). *Acta Cryst.* A**50**, 644–646.

Klug, A. & Franklin, R. E. (1958). *Discuss. Faraday Soc.* **25**, 104–110.

Makowski, L. (1978). *J. Appl. Cryst.* **11**, 273–283.

Makowski, L. (1982). *J. Appl. Cryst.* **15**, 546–557.

Millane, R. P. (1988). *Crystallographic Computing 4: Techniques and New Technologies*, edited by N. W. Isaacs & M. R. Taylor, pp. 169–186. Oxford University Press.

Millane, R. P. & Arnott, S. (1986). *J. Macromol. Sci. Phys.* **24**, 193–227.

Millane, R. P. & Stroud, W. J. (1991). *Int. J. Biol. Macromol.* **13**, 202–208.

Miller, A. & Parry, D. A. D. (1974). *Polymer*, **15**, 706–712.

Park, H., Arnott, S., Chandrasekaran, R., Millane, R. P. & Campagnari, F. (1987). *J. Mol. Biol.* **197**, 513–523.

Stroud, W. J. & Millane, R. P. (1995*a*). *Acta Cryst.* A**51**, 771–790.

Stroud, W. J. & Millane, R. P. (1995*b*). *Acta Cryst.* A**51**, 790–800.

Stroud, W. J. & Millane, R. P. (1996). *Proc. R. Soc. London Ser. A*, **452**, 151–173.

Suzuki, E., Fraser, R. D. B., Macrae, T. P. & Rowlands, R. J. (1980). *Fiber Diffraction Methods*, edited by A. D. French & K. H. Gardner, pp. 61–67. *ACS Symposium Series*, Vol. 141. Washington: American Chemical Society.

Tanaka, S. & Naya, S. (1969). *J. Phys. Soc. Jpn*, **26**, 982–993.

Welberry, T. R. (1985). *Rep. Prog. Phys.* **48**, 1543–1593.

Welberry, T. R. & Carroll, C. E. (1982). *Acta Cryst.* A**38**, 761–772.

Welberry, T. R. & Carroll, C. E. (1983). *Acta Cryst.* A**39**, 233–245.

Welberry, T. R., Miller, G. H. & Carroll, C. E. (1980). *Acta Cryst.* A**36**, 921–929.